

Characterising superconducting filters using residual microwave background

J. S. Lehtinen, E. Mykkänen, A. Kemppinen, and A. J. Manninen

VTT Technical Research Centre of Finland, Centre for Metrology MIKES, P.O. Box 1000, FI-02044 VTT, Finland

D. Golubev

Department of Applied Physics, Aalto University, P.O. Box 13500, FI-00076 Aalto, Finland

S. V. Lotkhov

Physikalisch-Technische Bundesanstalt, 38116 Braunschweig, Germany

(Dated: April 27, 2022)

A normal metal - superconductor hybrid single-electron trap with tunable barrier is utilized as a tool for spectrum analysis at the extremely low signal levels, using only well filtered cryogenic microwave background as a photon source in the frequency range from about 50 to 210 GHz. We probe millimeter wave propagation in two superconducting systems: a Josephson junction array around its plasma frequency, and a superconducting titanium film in the limit when the photon energies are larger than the superconducting energy gap. This regime is relevant for improving the performance of cryogenic quantum devices but is hard to access with conventional techniques. We show that relatively simple models can be used to describe the essential properties of the studied components.

I. INTRODUCTION

Interactions between photons and superconducting quantum systems are of two-fold interest: Those can be directly utilized in circuit quantum electrodynamics^{1,2} or, on the other hand, background photon emission e.g. from the warmer parts of the cryostat can be detrimental to the operation of quantum devices.³⁻⁶

Typical energy level spacing in a superconducting quantum device corresponds to the energy of a microwave or millimeter wave photon, which is significantly larger than thermal energy $k_B T$ at temperatures below 100 mK. The lowest microwave background levels have been obtained in experiments that combine on-chip filters with a low-noise sample stage having efficient radiation shielding and signal-line filtering.^{3,7} A variety of different on-chip filter elements have been used, including ground planes,^{8,9} thin-film resistors,^{10,11} and superconducting quantum interference device (SQUID) arrays as tunable impedance environment^{12,13} and non-uniform complex arrays as filters.^{14,15}

We have used the SINIS [S=superconductor (Al), I=insulator (AlO_x), N=normal metal (AuPd)] trap as an on-chip millimeter wave detector to study spectral transmission of two stages of on-chip filters: a Josephson array filter (JAF) and a resistive transmission line filter (RCF). Since millimeter waves can generate a significant amount of quasiparticles in both studied systems, thus altering their response, it is beneficial to study them at the lowest possible signal levels that can be reached in cryogenic experiments. Our signal source is simply the electromagnetic background of a sample chamber with efficient signal-line filtering and two nested shields,^{3,4,7} and we measure the rate of events caused by millimeter wave photons transmitted through the filters and absorbed by an on-chip detector.

II. PHOTON DETECTOR

Even as all quantum devices are extremely sensitive to environment fluctuations, the effects of microwave photons are rarely straightforward. Radiation shielding and filtering, or lack thereof, can be observed indirectly by any quantum device, but generally this does not provide quantitative information. Here with aid of sophisticated but well established data analysis we demonstrate the possibility to utilize a SINIS single-electron trap (Fig. 1a) as a tunable barrier single-photon detector^{11,16,17} and a tool for very low signal level spectrum analysis. For the trap, photon-assisted tunneling^{9,18,19} is the dominant electron transport mechanism, since both single- and two-electron inelastic tunneling processes can be efficiently eliminated by the Bardeen-Cooper-Schrieffer (BCS) energy gap and Coulomb blockade.^{20,21}

When a photon absorption occurs, the charge state of the normal metal island of the SINIS single-electron trap, n_1 (Figs. 1a and 1b), first changes by one but relaxes back to the original state by tunneling much faster than our measurement bandwidth. Therefore, we effectively see electron tunneling between the trap node and the superconducting reservoir electrode. The charge state of the trap is measured with a capacitively-coupled SINIS single-electron transistor functioning as an electrometer.¹⁶ Voltages V_s and V_g are applied to the control electrodes to tune the potentials of the superconducting trap node and the normal-metal island of the SINIS trap so that two charge states of the trap node, $n_2 = n, n+1$, are degenerate, but a change of n_1 requires extra energy from a photon. The relaxation of n_1 can occur in either direction with equal probability, so that half of the photon absorption events change n_2 and can be detected.

A significant benefit of the SINIS trap as a microwave photon detector is that the threshold energy of photon

assisted tunneling can be tuned between $\delta E = \Delta_{\text{Al}}$ and $\delta E = \Delta_{\text{Al}} + E_c$, where $\Delta_{\text{Al}} \approx 220 \mu\text{eV}$ and $E_c \approx 650 \mu\text{eV}$ are the BCS gap of aluminum and the charging energy of the island, respectively. The corresponding range for threshold frequencies $f_{\text{th}} = \delta E/h$ is between about 50 GHz and 210 GHz (h is the Planck constant). The overall quantum efficiency is low because of inevitable impedance mismatch between the high impedance tunnel junctions and the environment.

Typical time trace data of the electrometer is shown in Fig. 1c. The electrometer was symmetrically current biased with I_d between 5 to 20 pA, and the resulting voltage V_d was measured with a differential voltage amplifier and a digital voltmeter. Utilizing only small detector currents limits the generation of excess random telegraph noise which could be a source of significant error signals in the measurement of the microwave background.³ The measured time constant of the electrometer, about 1.7 ms, is limited by its resistance and the capacitance of the measurement lines. The effect of missed events on the measured electron hold times τ due to the bandwidth was corrected according to Naaman and Aumentado²². At low frequencies, the measurement band is limited by the background charge stability and the time required to obtain sufficient statistics. In practice, we are limited to $\tau \lesssim 100$ s, but hold times longer than half an hour were observed with the highest threshold energies.

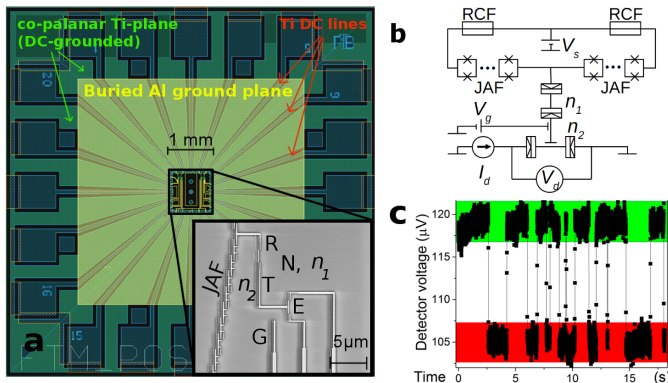


FIG. 1. a) Overview image of the sample with the hybrid titanium transmission line filter (RCF) with buried ground-plane. Inset: A scanning electron micrograph of the Josephson array filter (JAF) and the SINIS trap detector. Millimeter wave photons cause transport of individual electrons between the superconducting reservoir electrode (R) and trap node (T) via the normal metal island (N) of the SINIS single-electron trap, and the change of the charge state (n_2) of T is detected by a SINIS single-electron transistor that acts as an electrometer (E). b) A scheme of the device and the measurement circuit. c) Typical two-state single-electron charge fluctuation of the SINIS trap, when the charge states $n_2 = n$ (red) and $n_2 = n + 1$ (green) are degenerate. The trace shows the output voltage V_d of the SINIS electrometer that is biased with a current $I_d = 10$ pA at $T = 32$ mK.

To obtain spectral information, the photon assisted tunneling (PAT) rate Γ and thus the electron hold time

τ of the trap node needs to be attained in terms of background noise spectrum. For this purpose the probability density theory was used.¹⁸ The tunneling rate through a NIS junction is

$$\Gamma(\delta E) = 1/\tau(\delta E) = \frac{1}{e^2 R_T} \times \int_{-\infty}^{\infty} dE dE' n_S(E) f(T, E) [1 - f(T, E' + \delta E)] P(E - E'), \quad (1)$$

where e is the elementary charge, T is the electron temperature, R_T is the tunneling resistance of the junction, $n_S(E)$ is the BCS density of states, $f(E)$ is the Fermi function, and $P(E)$ is the probability density to emit or absorb energy E in the tunneling process. The effect of the charging energy is described by the electrostatic energy change δE . For simplicity, this equation is expressed for tunneling from the superconductor to the normal metal, but the opposite process can be described in a similar way.

Neglecting quantum fluctuations, $P(E)$ can be written in terms of the spectral noise density at the detector, $S_{V,\text{det}}(\omega)$, as²³

$$P(E) = \frac{1}{2\pi\hbar} \int_{-\infty}^{\infty} dt \exp\left(\frac{iEt}{\hbar}\right) \times \exp\left(\frac{2\pi}{R_q \hbar} \int_0^{\infty} d\omega \frac{S_{V,\text{det}}(\omega)}{\omega^2} \cos(\omega t - 1)\right), \quad (2)$$

where $R_q = h/e^2$ is the resistance quantum, $\hbar = h/(2\pi)$, and $\omega = 2\pi f$ is the angular frequency of the noise. In the weak noise limit, the second exponential term can be approximated with first order expansion which is valid at energies above about $k_B T$.²³ To cover the whole energy range, we approximate $P(E)$ with a Dirac delta function at energies below the boundary value $\epsilon_0 \sim k_B T$, and use a piecewise model

$$P(E) = \begin{cases} \alpha \delta(E) & , E < \epsilon_0 \\ \frac{\pi S_{V,\text{det}}(E/\hbar)}{R_q E^2} & , E \geq \epsilon_0 \end{cases} \quad (3)$$

where α is a normalization factor close to one.

III. PHOTON SOURCE

As a source of millimeter waves in our experiment we used thermal radiation from warmer parts of the cryostat. It is a major source of microwave background for cryogenic environments at $T < 100$ mK. Its effect on quantum electronic devices is often modelled using fluctuation-dissipation theorem with an electromagnetic environment, e.g. a resistor, at an elevated temperature.^{3,9,16,24-26} We have used a slightly different approach and modelled the spectral noise density that couples to the chip, $S_{V,\text{in}}(\omega)$, using Planck radiation law for a black body at elevated temperature. For our experiment this model is virtually indistinguishable from the

fluctuation-dissipation model with a resistor at elevated temperature. In the sensitive range of our detector, both models yield almost identical noise spectra with only a small difference in the temperature of the radiating object.

Starting from the Planck radiation law, we write the spectral voltage noise density, originating from the photon bath in the sample chamber, as

$$S_{V,\text{in}} = \beta_0 S_P(\omega) = \beta_0 \frac{\hbar\omega^3}{4\pi^3 c^2} \frac{1}{\exp(\frac{\hbar\omega}{k_B T_P}) - 1}, \quad (4)$$

where $S_P(\omega)$ is the power spectrum of the microwave radiation observed at the chip, c is the speed of light, k_B is the Boltzmann constant, T_P is the temperature of the black body emitter of the model, and β_0 is the coupling coefficient between the black body source and the chip and in the model is a frequency-independent coefficient having dimensions of Ωm^2 . In principle β_0 could be used to compare the shielding and filtering levels of cryogenic setups even though its origin cannot be fully distinguished.

One should note that even though both the fluctuation-dissipation theorem and the Planck radiation law have exact physical origins, in this context they should be considered as phenomenological models. Such thermal distributions are only a crude approximation as the signal at the sample chamber has already penetrated the sample stage shields and/or signal line filters. Also in a realistic case the black body emitter temperature should have distribution based on the cryostat construction, i.e. the noise is not emitted by objects with the same temperature. Yet the collection of data (see Fig. 4.4 of Saira²⁷) from multiple experiments indicate roughly exponential decrease of the microwave background as a function frequency.^{3,9,16,26} We find the Planck model suitably simple with only two fitting parameters, of which β_0 affects only the overall magnitude of the noise, and T_P also the slope of the exponential decrease. It is important also to understand the phenomenological nature of T_P . Both the sample chamber radiation shields, radiation coupling to the chip and the on-chip transmission lines (see Sec. V) between bonding pads and the detector affect the frequency dependence of the noise, and thus the effective T_P seen by the detector.

IV. EXPERIMENTAL RESULTS

In our experiments, photons from the sample chamber were transmitted through the RCF and JAF filters and became absorbed in the detector, causing PAT events in the SINIS trap, see Figs. 1a and 1b. Electron hold times of the trap node were measured in different environment conditions (external magnetic field B and bath temperature T) to determine attenuation properties of the filters. Spectral information was obtained by repeating the measurements with different values of threshold frequency of

the trap f_{th} , which is the minimum frequency that the photon must have to be able to cause a PAT event in the trap. The value of f_{th} can be adjusted by voltages V_s and V_g but not measured directly. Results of the experiment are shown in Fig. 2, which also includes simulation results based on theoretical models described in Sec. V. The data of Figs. 2a and 2b were mainly used for studies of JAF and RCF, respectively, and the determination of the value of f_{th} for different data sets was mainly based on the data of Fig. 2d.

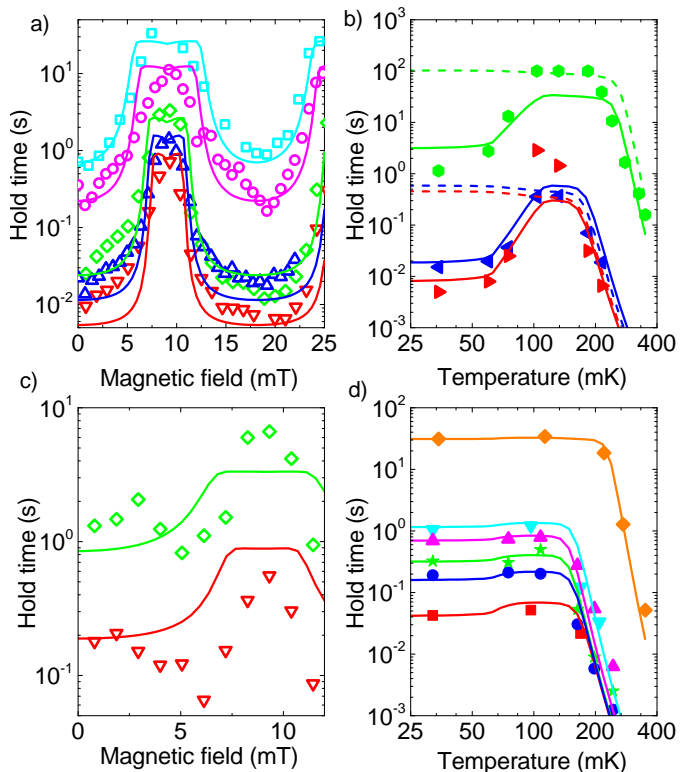


FIG. 2. Experimental results for the electron hold times of the SINIS trap in different temperatures and magnetic fields and with different values of f_{th} . In each panel, the solid and dashed lines are simulation results based on $P(E)$ theory and circuit models (see the text). a) Magnetic field dependence at base temperature $T = 32$ mK. Different symbols correspond to different values of f_{th} : red down-pointing triangles 109 GHz, blue triangles 117 GHz, green diamonds 128 GHz, magenta spheres 150 GHz, and cyan squares 161 GHz. b) Temperature dependence at $B = 0$ with $f_{\text{th}} = 109$ GHz (red right-pointing triangles), 121 GHz (blue left-pointing triangles), and 173 GHz (green spheres). c) Magnetic field dependence at elevated temperature $T = 110$ mK with $f_{\text{th}} = 109$ GHz (red down-pointing triangles) and 128 GHz (green diamonds). d) Temperature dependence at $B = 8$ mT which corresponds to $\Phi = \Phi_0/2$ for the SQUIDs of the JAF filter. Different symbols correspond to different values of f_{th} : 73 GHz (red squares), 93 GHz (blue spheres), 101 GHz (green stars), 109 GHz (magenta triangles), 113 GHz (cyan down-pointing triangles) and 164 GHz (orange diamonds).

Magnetic field dependence of the hold time at the base

temperature of the cryostat, about 32 mK, is presented in Fig. 2a. Different symbols correspond to different values of f_{th} . The observed B -dependent variation of the hold time of the trap between $\Phi = 0$ and $\Phi = \Phi_0/2$ is about two orders of magnitude. The Josephson inductance of the SQUIDs in the JAF is a periodic function of B , with a period of 16 mT that corresponds to a magnetic flux $\Phi = \Phi_0$ through the SQUID loops in our geometry, where $\Phi_0 = h/(2e)$ is the magnetic flux quantum. This adjustable inductance of the JAF can explain the strong B -dependence of the hold time (see Sec. VB).

Figure 2b shows temperature dependence of the hold time at $B = 0$, which corresponds to the minimum attenuation of JAF. At temperatures above about 200 mK, the hold time decreases exponentially as a function of T due to thermally excited tunneling events in the SINIS trap. At lower temperatures the hold time is determined by the frequency of the photon assisted tunneling events. A surprisingly large decrease in the hold time was observed with all studied f_{th} when temperature was decreased below about 100 mK. This is equal or very close to the superconducting transition temperature T_c of the RCF, which is a resistive transmission line in which titanium film with $T_c \simeq 110$ mK is used as resistive material. The threshold frequencies were much higher than the pair-breaking frequency of titanium, $2\Delta_{\text{Ti}}/h \sim 34$ GHz, where $\Delta_{\text{Ti}} = 70 \mu\text{eV}$ is the BCS energy gap of titanium, and thus the attenuation of RCF was expected to have only weak temperature dependence and a small change at T_c of Ti film.

As discussed in Sec. VA, this behaviour cannot be described by the typical Mattis-Bardeen model for high frequency propagation in a superconducting film.²⁸ On the other hand, we expect no temperature dependence of the JAF below $T = 100$ mK, because it is extremely difficult to suppress the quasiparticle density of superconducting Al structures below the effective temperature of 100 mK.³ In Sec. VA we find that the Werthamer model for uniform array of Josephson junctions describes better the high frequency propagation in our highly disordered superconducting Ti-films.²⁹

Figure 2c demonstrates that at $T = 110$ mK, the B -dependent variation of the hold time (factor of 4) is much smaller than at $T = 32$ mK (factor of 100). This is not surprising since RCF is a much more effective filter at $T = 110$ mK than at lower temperatures (see Fig. 2b), and other effects, especially noise photons that bypass both filters, become significant. Finally, Fig. 2d shows the temperature dependence of the hold time at $B = 8$ mT. In this case, the JAF is an efficient filter and tunneling events are dominated by noise photons that bypass the filters, and hence the effect of RCF on the hold time is very small or negligible. In the PAT-dominated low temperature limit, the hold time is almost T -independent for all measured f_{th} . When temperature is sufficiently high to cause thermally excited tunneling in the trap, an exponential decrease of the hold time is observed. This decrease is independent of microwave

background noise, and these data are used in Sec. V to determine the values of δE and f_{th} for each set of measurements.

V. ANALYSIS

Our experimental data presented in Fig. 2 consist of electron hold times τ measured in different temperatures and magnetic fields. In data analysis, $\tau = 1/\Gamma$ is calculated using Eq. (1) with the approximate form of Eq. (3) for $P(E)$. The detector is sensitive to the average noise $S_{V,\text{det}}(\omega)$ between its trap node and the superconducting reservoir electrode (see Fig. 1a). $S_{V,\text{det}}(\omega)$ in Eq. (3) is obtained from the spectral noise voltage picked up by the chip, $S_{V,\text{in}}(\omega)$ (Eq. (4)), using the circuit model described in Fig. 3a. The noise is filtered by the B -dependent JAF (transmission coefficient $\kappa_{\text{JAF}}(B, \omega)$) and the T -dependent RCF (transmission coefficient $\kappa_{\text{RCF}}(T, \omega)$) connected in series. The total transmission through these series filter elements $\kappa_F(T, B, \omega) = \kappa_{\text{RCF}}(T, \omega)\kappa_{\text{JAF}}(B, \omega)$ depends on temperature, magnetic field, and frequency. The models for the filter elements RCF and JAF are discussed in separate sections, Sec. VA and Sec. VB, respectively.

When the filtering is efficient, i.e. κ_F is small, the noise coupled by stray capacitances from the other nearby electrodes, κ_0 (see Fig. 3a), dominates. We first tried using frequency independent κ_0 , but noticed that then the fits to the experimental data would have required different values of T_P for the noise coupled to the input of the RCF filter and for that coupled directly to the detector. A plausible explanation is that on-chip transmission lines change the frequency response in the following way.

All signal lines coming to the sample region have essentially similar transmission line filters as the RCF that is connected to the JAF and the trap, see Fig. 1a. However, there is a 1 mm \times 1 mm region around the detector where each line continues about the distance $d \approx 0.5$ mm without the ground plane. We assume that the noise bypassing the filters is dominated by microwave photons entering this region, and we model its coupling to the detector with a lumped element RC transmission line.

We calculate frequency-dependent transmission coefficients $\kappa(\omega)$ for lossy lumped element transmission lines using Telegraphers equations, see for example Pozar³⁰. Only dissipative losses of the conductor are taken into account as those are considered to be the dominating signal attenuation mechanism for our filters, and we write

$$\kappa(\omega) = V_{\text{out}}(\omega)/V_{\text{in}}(\omega) = e^{-\text{Re}[\gamma(\omega)]l}, \quad (5)$$

where V_{in} and V_{out} are voltages in the input and output ports of the filter, respectively, l is the length of the transmission line, and $\gamma = \sqrt{i\omega C'_{\text{shunt}} Z'_{\text{series}}}$ is the complex propagation coefficient, where Z'_{series} is the series impedance and C'_{shunt} the shunt capacitance per unit length for the transmission line.

Using Eq. (5) we obtain the transmission coefficient for the signal lines without the ground plane $\kappa_0 = A \exp(-\text{Re}[\sqrt{i\omega C' R'}]d)$. Coupling of the microwave background noise into the signal lines is weaker in the middle of the chip than on the bonding pads outside the ground plane, and that difference is quantified by the fitting parameter $A < 1$. In the frequency range of our experiments, the product $\kappa_0 S_{V,\text{in}}$ has a shape very close to the Planck spectrum of Eq. (4) but with a different black body temperature T_P . The best fits to the data are obtained using realistic parameters $R' = 4.5 \text{ } \Omega/\mu\text{m}$ and $C' = 300 \text{ aF}/\mu\text{m}$ for resistance and capacitance per length, respectively, and $A \approx 0.1$.

The relation between voltage noise density entering the chip, $S_{V,\text{in}}$ in Eq. (4), and reaching the detector, $S_{V,\text{det}}$, is described by the transmission coefficient $\kappa(T, B, \omega)$:

$$S_{V,\text{det}} = \kappa S_{V,\text{in}} = [\kappa_{\text{JAF}}(B, \omega)\kappa_{\text{RCF}}(T, \omega) + \kappa_0(\omega)] S_{V,\text{in}}. \quad (6)$$

Even though the simulations of Fig. 2 are based on this relatively complicated overall transmission coefficient (6), we note that κ_{JAF} , κ_{RCF} , and κ_0 each depend mainly on a single set of measurements: Figs. 2a, 2b, and 2d, respectively. This helped us to ensure that unambiguous values were obtained for the fitting parameters.

The starting point for the data analysis are the results of Fig. 2d, which were measured when the JAF had large attenuation and the PAT effects of the detector were dominated by the noise that had bypassed the filters via the transmission channel κ_0 . The measurements were done with 6 values of f_{th} , whose value for each data set was determined from fits to the data. In the first iteration, the transmission through the filters was not taken into account at all, but the final results presented as solid lines in Fig. 2d are calculated with the full model of Fig. 3a, including the models for the RCF and JAF.

From simultaneous fits to Eq. (1) for several data sets with different values of f_{th} , each extending from the PAT-dominated low-temperature limit up to temperatures where thermal excitations cause exponential decrease of the hold time, unambiguous values $T_P = 1.5 \text{ K}$ and $\beta_0 = 2 \times 10^{-2} \text{ } \Omega\text{m}^2$ for the fitting parameters of Eqs. (4) and (6) could be obtained, as well as for the values of f_{th} for each data set. These results were also used to determine the values of f_{th} in the measurements of Figs. 2a-c.

The green line and green symbols in the top panel of Fig. 3b show the relation between the low-temperature electron hold time and threshold frequency f_{th} of the trap for the experimental case of Fig. 2d. The bottom panel shows the corresponding spectral noise density near the detector as a function of frequency. The other lines in Fig. 3b correspond to experimental conditions where the on-chip filters are effective, and they have been calculated using Eq. (1) with Eqs. (3) and (4), and applying the filter models of Sections V A and V B in Eq. (6). The sensitive range of our SINIS detector is shaded with gray.

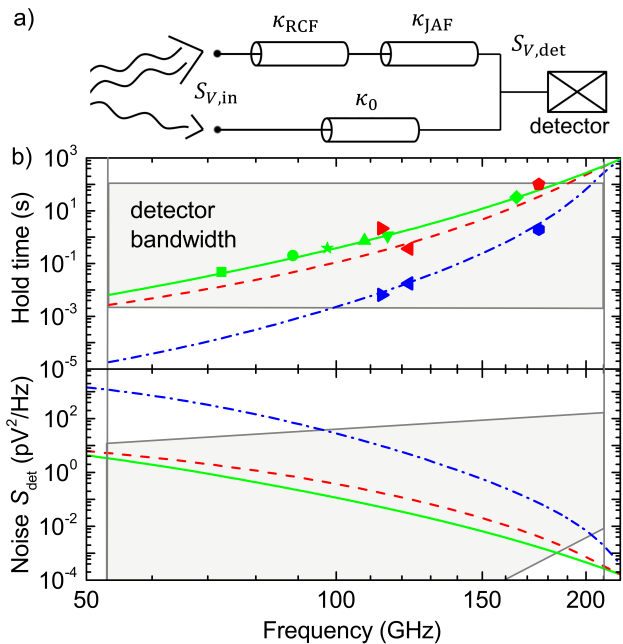


FIG. 3. a) Model for noise propagation in the circuit. Microwave photons of the sample chamber cause voltage noise at the chip $S_{V,\text{in}}$. It is transmitted to the detector via two parallel channels, through the series filter elements JAF and RCF or through electrodes near the detector without ground plane (κ_0). b) Top panel: The relation between the electron hold time τ and threshold frequency f_{th} of the SINIS detector in different environment conditions: $B = 8 \text{ mT}$ and $T = 32 \text{ mK}$ (green solid line), $B = 0$ and $T > 100 \text{ mK}$ (red dashed line), and $B = 0$ and $T < 50 \text{ mK}$ (blue dash-dotted line). The lines are based on fits of experimental data to $P(E)$ theory, modelling $S_{V,\text{det}}(\omega)$ in different experimental conditions using Planck radiation and the coupling scheme of (a). The measured hold time data are marked with similar symbols as in Fig. 2 but with the same colour as the corresponding line. Bottom panel: Spectral density of microwave radiation reaching the detector $S_{V,\text{det}}$ in different experimental conditions using the same notation as in the top panel. The sensitive range of our SINIS detector is indicated with gray shading.

A. Resistive transmission line

As shown in the large-scale image of Fig. 1a, the resistive transmission line filters (RCF) consist of a titanium electrode which is capacitively coupled to a buried aluminium ground plane. The length of the filter, about 3.5 mm, is comparable to the wavelength of microwaves in the frequency range of our experiments. The Ti layer is highly resistive ($\sim 100 \text{ } \Omega/\square$) in the normal state, i.e. when either temperature or magnetic field is above the critical value of about 110 mK or 40 mT, respectively. The microwave attenuation of RCF was not expected to change much at the superconducting transition of Ti, but the experiments of Fig. 3b show that the hold time of electrons in the SINIS detector increases by two orders

of magnitude when temperature decreases below T_c of titanium film, about 110 mK.

First we demonstrate that the temperature dependence of the RCF cannot be explained by the theory formulated by Mattis and Bardeen²⁸ which is a well

$$\frac{\sigma_{\text{MB1}}}{\sigma_N} = \frac{2}{\hbar\omega} \int_{\Delta_{\text{Ti}}}^{\infty} \frac{[f(E) - f(E + \hbar\omega)](E^2 + \Delta_{\text{Ti}}^2 + \hbar\omega E)}{\sqrt{E^2 - \Delta_{\text{Ti}}^2} \sqrt{(E + \hbar\omega)^2 - \Delta_{\text{Ti}}^2}} dE + \frac{1}{\hbar\omega} \int_{\Delta_{\text{Ti}} - \hbar\omega}^{-\Delta_{\text{Ti}}} \frac{[1 - 2f(E + \hbar\omega)](E^2 + \Delta_{\text{Ti}}^2 + \hbar\omega E)}{\sqrt{E^2 - \Delta_{\text{Ti}}^2} \sqrt{(E + \hbar\omega)^2 - \Delta_{\text{Ti}}^2}} dE \quad (7)$$

is a dissipative part with thermal and photon excited quasiparticles and

$$\frac{\sigma_{\text{MB2}}}{\sigma_N} = \frac{1}{\hbar\omega} \int_{-\Delta_{\text{Ti}}}^{\Delta_{\text{Ti}}} \frac{[1 - 2f(E + \hbar\omega)](E^2 + \Delta_{\text{Ti}}^2 + \hbar\omega E)}{\sqrt{E^2 - \Delta_{\text{Ti}}^2} \sqrt{(E + \hbar\omega)^2 - \Delta_{\text{Ti}}^2}} dE \quad (8)$$

is the dissipationless superfluid response. In the equations above, σ_N is the normal-state conductivity of the titanium film. We modelled the RCF in superconducting state as a finite length lumped element RLC transmission line³⁰ with resistance per unit length $R'_S(\omega, T) = R'_N/(\sigma_{\text{MB1}}/\sigma_N)$ and inductance per unit length $L'_S(\omega, T) = (R'_N/\omega)/(\sigma_{\text{MB2}}/\sigma_N)$ from parallel quasiparticle and Cooper pair channels, respectively (see Fig. 4a, left). Here $R'_N = 505 \Omega/\text{mm}$ is the normal state resistance of the Ti film per unit length obtained from an independent measurement. The fits to our data yield $C'_{\text{gp}} = 0.2 \text{ pF}/\text{mm}$ as the capacitance per unit length between the Ti film and the buried ground plane, which is in reasonable agreement with the value of $1 \text{ pF}/\text{mm}$ estimated from geometry.

The superconducting transition of a thin nonhomogeneous film has a finite width as a function of temperature due to local variations of T_c . In the model this was taken into account by dividing the transmission line to superconducting and normal-metal parts connected in series, with temperature dependent lengths $l_S(T)$ and $l_N(T)$, respectively, as shown in Fig. 4a. Temperature dependencies of $l_S(T)$ and $l_N(T)$ relative to the total length $l = 3.5 \text{ mm}$ of the transmission line were obtained from the temperature dependence of the dc resistance of the RCF near T_c of Ti film shown in the bottom panel of Fig. 4b.

The model described above and the circuit in Fig. 4a were used to calculate the transmission coefficient (Eq. (5)) of the resistive transmission line filter

$$\kappa_{\text{RCF}}(T, \omega) = \exp\left(-\text{Re}\left[\sqrt{(i\omega C'_{\text{gp}} R'_N)}\right] l_N(T) - \text{Re}\left[\sqrt{(i\omega C'_{\text{gp}} \frac{i\omega L'_S(\omega, T) R'_S(\omega, T)}{i\omega L'_S(\omega, T) + R'_S(\omega, T)})} l_S(T)\right]\right), \quad (9)$$

and that was applied in Eqs. (6), (3) and (1) to simulate the electron hold time of the detector as a function of temperature, assuming that JAF is temperature-independent below $\sim 110 \text{ mK}$. The dashed lines in Fig. 2b

established model for microwave frequency propagation in superconducting films. Frequency dependent complex conductivity of a superconductor can be written as $\sigma_{\text{MB}}(\omega, T) = \sigma_{\text{MB1}}(\omega, T) - i\sigma_{\text{MB2}}(\omega, T)$, where

are results of the Mattis-Bardeen model with realistic parameter values. As can be seen, this model does not explain the observed decrease of the hold time when temperature is decreased below T_c of Ti film.

Instead, the temperature dependence can be explained at least semi-quantitatively by the disorder of the thin Ti film evaporated in presence of residual oxygen. We assume that the Ti film consists of weakly connected grains that form Josephson junctions. To simplify this complex circuit, we approximate it as an array of identical Josephson junctions with high-frequency response derived by Werthamer.²⁹ Writing the complex conductivity as previously for quasiparticle and Cooper pair channels, $\sigma_W(\omega, T) = \sigma_{W1}(\omega, T) - i\sigma_{W2}(\omega, T)$, and assuming $\hbar\omega > \Delta_{\text{Ti}}$, we get

$$\frac{\sigma_{W1}}{\sigma_N} = \frac{\Delta_{\text{Ti}}}{\hbar\omega} \left[\frac{\hbar\omega}{\Delta_{\text{Ti}}} E\left(\sqrt{1 - \frac{\Delta_{\text{Ti}}^2}{\hbar^2\omega^2}}\right) - \frac{\Delta_{\text{Ti}}}{\hbar\omega} K\left(\sqrt{1 - \frac{\Delta_{\text{Ti}}^2}{\hbar^2\omega^2}}\right) \right] \quad (10)$$

$$\frac{\sigma_{W2}}{\sigma_N} = \frac{\Delta_{\text{Ti}}}{\hbar\omega} \left[\frac{\hbar\omega}{\Delta_{\text{Ti}}} \left(E\left(\frac{\Delta_{\text{Ti}}}{\hbar\omega}\right) - K\left(\frac{\Delta_{\text{Ti}}}{\hbar\omega}\right) \right) + \pi \right], \quad (11)$$

where the functions K and E are the elliptic integrals. The result above is strictly valid in zero-temperature limit, but we use it as an approximation on the whole temperature range, assuming only temperature dependence for the energy gap of titanium calculated from BCS theory. However, only the low-temperature limit and normal-state situation are important for our conclusions.

We again modelled the superconducting parts of the RCF as an RLC transmission line (Eq. 9) with the same parameters as above but using values from Eqs. (10) and (11), $R'_S(\omega, T) = R'_N/(\sigma_{W1}/\sigma_N)$ and $L'_S(\omega, T) = (R'_N/\omega)/(\sigma_{W2}/\sigma_N)$, for resistance and inductance per unit length, respectively. The hold time of electrons in the SINIS trap was calculated as explained above, and the results shown using solid lines in Fig. 2b are in reasonable agreement with the experimental data. The temperature and frequency dependent attenuation

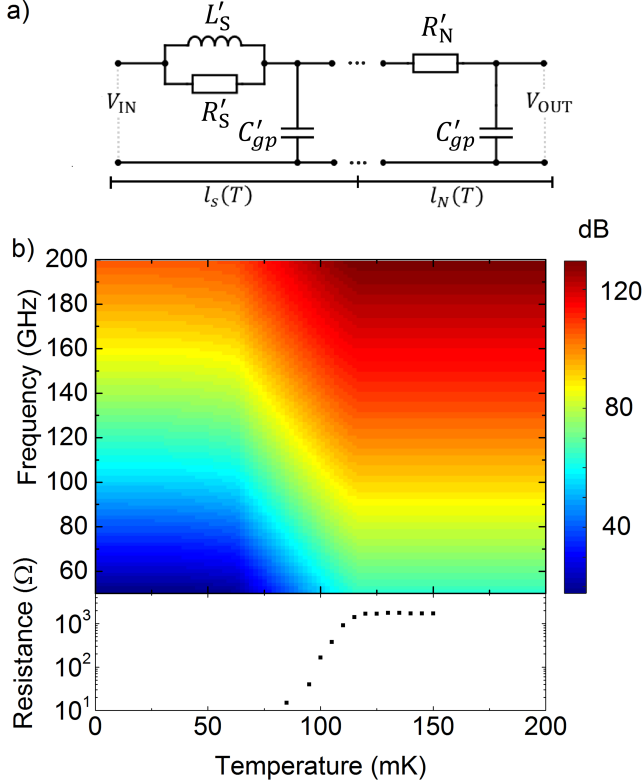


FIG. 4. a) The circuit model used for the RCF consisting of the superconducting (left) and normal-metal parts (right). b) Top panel shows attenuation $1/\kappa_{RCF}$ in decibel scale as a function of temperature and frequency for the RCF modelled using the Werthamer model²⁹ as explained in the text. The bottom panel shows the observed dc-resistance of the RCF as a function temperature.

$1/\kappa_{RCF}(\omega, T)$ calculated using this model is shown in the top panel of Fig. 4b.

B. Josephson array filter

The Josephson array filter (JAF) consists of two branches, with 5 and 35 aluminum SQUIDs in series, respectively (Fig. 1a). The effects studied in this work are dominated by the 5-SQUID branch. Its attenuation can be tuned by a magnetic field, since each SQUID of the JAF is effectively a tunable Josephson inductance element with

$$L_J(\Phi) = \Phi_0 / (2\pi I_c(\Phi)). \quad (12)$$

The critical current $I_c(\Phi) \simeq I_c(0) \cos(\pi\Phi/\Phi_0)$ has maxima and minima when the magnetic flux Φ through the SQUID loop is integer or half integer multiple of the flux quantum Φ_0 , respectively. The magnetic field that corresponds to Φ_0 in the SQUID loops of JAF is about 16 mT.

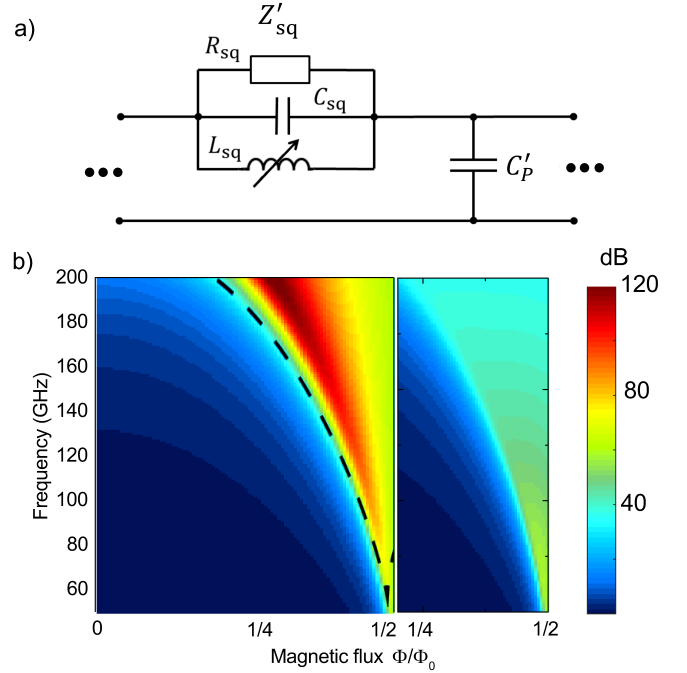


FIG. 5. a) The transmission line element used in analysing the Josephson array filter. b) Left panel: Attenuation $1/\kappa_{JAF}$ calculated for the JAF model at low temperature $T \ll 100$ mK as a function of magnetic flux Φ and frequency f . The plot covers the range of Φ from 0 to $\Phi_0/2$, but the attenuation is a periodic function of Φ with period $\Phi = \Phi_0$, and the range from $\Phi_0/2$ to Φ_0 is a mirror image of the range covered in the plot. When frequency and magnetic flux are above the region bounded by the black dashed line, experiments are dominated by the parasitic coupling κ_0 (see Fig. 3a) and the effects of JAF cannot be observed. Right panel: Additional attenuation of JAF when the effects of RCF and parasitic coupling are taken into account.

The frequency range of the SINIS trap detector, higher or comparable to the magnetic flux dependent plasma frequency of the SQUIDs $f_p \sim 20 - 200$ GHz, is a region that is hard to model theoretically. We have treated this complex system with a simplified model suitable for experimental work. The chain of the 5 SQUIDs of the JAF, with total length about $l_{chain} = 15 \mu\text{m}$, is treated as a lumped element RLC-transmission line circuit³⁰ shown in Fig. 3c. The model is similar to that used by Haviland *et al.*³¹ but takes into account transmission losses to make the model applicable above the plasma frequency. Each SQUID element consists of three parallel elements, kinetic inductance $L_{sq}(\Phi) = \Phi_0 / (2\pi I_c(\Phi))$, total junction capacitance $C_{sq} = 0.5$ fF and resistive damping term $R_{sq} = 10$ k Ω . Thus the SQUID impedance per unit length is

$$Z'_{sq} = \left(i\omega C_{sq} + \frac{1}{i\omega L_{sq}} + \frac{1}{R_{sq}} \right)^{-1} / l_{sq}, \quad (13)$$

where $l_{sq} = 3 \mu\text{m}$ is the length of one SQUID. The capac-

itance per unit length between the transmission line and environment is estimated to be about $C'_p = 300$ aF/ μm . The critical current of the Josephson junctions at $\Phi = 0$, $I_c(0) = 0.49$ μA , was used as a fitting parameter. The best fits were obtained with critical current 2.7 times the value estimated from the measured junction resistance $R_J = 2.3$ k Ω and superconducting energy gap $\Delta_{\text{Al}} = 220$ μeV using the Ambegaokar-Baratoff relation.³² The damping resistances are considered to originate from the dielectric losses^{33,34} and would correspond to a loss tangent $\tan \delta \approx 0.1$, which is plausible when considering the very low signal level and the high photon frequency. The junction capacitance was estimated from the total junction area of each SQUID $A_j = 2 \times 0.01$ μm^2 , oxide thickness $d = 1.5$ nm, and relative permittivity $\epsilon = 4.5$.

Transmission coefficient of the JAF, using Eq. (5) is

$$\kappa_{\text{JAF}}(B) = \exp \left[-\text{Re} \left[\sqrt{i\omega C'_p Z'_{\text{sq}}} \right] l_{\text{chain}} \right], \quad (14)$$

which depends on magnetic field via $L_{\text{sq}}(\Phi)$, and it was used in Eqs. (6), (3) and (1) to simulate magnetic field dependence of the hold time. Reasonably good agreement with the data in Fig. 2a at all f_{th} was obtained. The JAF attenuation $1/\kappa_{\text{JAF}}$ based on the model is presented in the left panel of Fig. 5b. The maximum attenuation is not reached at $\Phi = \Phi_0/2$ but at a value of Φ corresponding the LC-resonance (plasma frequency) of the SQUID, which for higher frequencies occurs at smaller values of Φ . This leads to widening of the magnetic field range where the attenuation is high as the f_{th} increases. The effect can be observed in the experimental results of Fig. 2a.

However, the resonances themselves cannot be observed directly in the experiment, since the parasitic coupling, κ_0 , dominates when JAF has large attenuation. The region where κ_0 dominates is marked in the left panel of Fig. 5b with a dashed line. The right panel of Fig. 5b demonstrates the effective filtering performance of JAF when the leakage caused by parasitic coupling κ_0 is taken into account. The ratio $\kappa/\kappa_{\text{wo-JAF}} = (\kappa_{\text{JAF}}\kappa_{\text{RCF}} + \kappa_0)/(1 \times \kappa_{\text{RCF}} + \kappa_0)$ calculated using the models of JAF, RCF and κ_0 , is plotted as a function of magnetic flux and frequency in the low-temperature limit, where the attenuation of RCF is not maximised. Here κ is the transmission coefficient for the complete system (Eq. 6) when JAF is in use, and $\kappa_{\text{wo-JAF}}$ is the transmission coefficient when JAF is shunted with perfect transmission ($\kappa = 1$).

In spite of the simplicity of the model with respect to the physical complexity of the system, the uncertainty of the experimentally defined parameters and the unavoidable structural non-idealities, the fits in Fig. 2a are in good agreement with experimental results. The model explains both the magnitude of the B -dependent modulation of the hold times with different f_{th} and the widening of the magnetic field range of high attenuation at higher f_{th} . However the model is phenomenological and the strict origin of parameters as well as the suitability

of the transmission line model for the system should be considered critically. Better validation of the model requires experiments with more simplified systems, without the RC-filter, where the JAF attenuation would not be limited by κ_0 .

Finally, the full coupling model of Fig. 3 also explains at least semi-quantitatively the result of Fig. 2c, i.e., much weaker magnetic field dependence of the hold time at $T = 110$ mK than at $T = 32$ mK (Fig. 2c). The reason is that at $T = 110$ mK the attenuation of RCF is large, which means that a considerable fraction of detected photons arrive via the B -independent parasitic coupling κ_0 in all magnetic fields, whereas at $T = 32$ mK the attenuation of RCF is much smaller and photons arrive the detector mainly via RCF and JAF, and κ_0 has an important contribution only in magnetic fields where the attenuation of JAF is high.

VI. CONCLUSIONS

We demonstrated that a single-electron trap excited by individual photons can be used to obtain spectral information of cryoelectronic devices at millimeter wave frequencies with extremely low signal levels. Our source of millimeter wave photons was the electromagnetic background in a well shielded and filtered sample chamber at temperature of about 30 mK. Our results are consistent with linearly attenuated Planck spectrum of a black-body emitter at 1.5 K before the filter elements.

Two series-connected elements used as cryogenic mm-wave filters, a 15- μm -long Josephson array filter (JAF) consisting of an array of aluminium SQUIDS, and a 3.5-mm-long resistive transmission line filter (RCF) made of titanium, were characterised. Both filters were effective attenuators for millimeter waves. When the mm-wave attenuation of JAF was tuned by a magnetic field, the hold time of electrons in the single-electron trap changed by two orders of magnitude. We demonstrated that even a simple circuit model, in spite of the theoretical complexity of the SQUID at frequencies comparable to the plasma frequency, is suitable for qualitative description of the millimeter wave transmission. In RCF, the mm-wave attenuation was observed to decrease considerably when temperature decreased below the superconducting transition temperature of titanium. The behaviour could be explained by Josephson coupling between weakly connected grains of the titanium film but not with conventional models.

We thank A. B. Zorin, J. Hassel, O.-P. Saira and V. F. Maisi for discussions. The research was financially supported by the Wihuri foundation (E.M.) and by the Academy of Finland (A.K., grant 259030). This work belongs to the Joint Research Project MICROPHOTON of the European Metrology Research Programme (EMRP). The EMRP is jointly funded by the EMRP participating countries within EURAMET and the European Union.

- ¹ A. Wallraff, A. Schuster, D. I. and Blais, L. Frunzio, R.-S. Huang, J. Majer, S. Kumar, G. S. M., and R. J. Schoelkopf, *Nature* **431**, 162 (2004).
- ² A. Blais, R.-S. Huang, A. Wallraff, S. M. Girvin, and R. J. Schoelkopf, *Phys. Rev. A* **69**, 062320 (2004).
- ³ O.-P. Saira, A. Kemppinen, V. F. Maisi, and J. P. Pekola, *Phys. Rev. B* **85**, 012504 (2012).
- ⁴ R. Barends, J. Wenner, M. Lenander, Y. Chen, R. C. Bialczak, J. Kelly, E. Lucero, P. O'Malley, M. Mariantoni, D. Sank, H. Wang, T. C. White, Y. Yin, J. Zhao, A. N. Cleland, J. M. Martinis, and J. J. A. Baselmans, *Applied Physics Letters* **99**, 113507 (2011), <http://dx.doi.org/10.1063/1.3638063>.
- ⁵ A. D. Corcoles, J. M. Chow, J. M. Gambetta, C. Rigetti, J. R. Rozen, G. A. Keefe, M. Beth Rothwell, M. B. Ketchen, and M. Steffen, *Applied Physics Letters* **99**, 181906 (2011), <http://dx.doi.org/10.1063/1.3658630>.
- ⁶ P. J. de Visser, J. J. A. Baselmans, S. J. C. Yates, P. Diener, A. Endo, and T. M. Klapwijk, *Applied Physics Letters* **100**, 162601 (2012), <http://dx.doi.org/10.1063/1.4704151>.
- ⁷ A. Kemppinen, S. V. Lotkhov, O.-P. Saira, A. B. Zorin, J. P. Pekola, and A. J. Manninen, *Appl. Phys. Lett.* **99**, 142106 (2011).
- ⁸ A. Steinbach, P. Joyez, A. Cottet, D. Esteve, M. H. Devoret, M. E. Huber, and J. M. Martinis, *Phys. Rev. Lett.* **87**, 137003 (2001).
- ⁹ J. P. Pekola, V. F. Maisi, S. Kafanov, N. Chekurov, A. Kemppinen, Y. A. Pashkin, O.-P. Saira, M. Möttönen, and J. S. Tsai, *Phys. Rev. Lett.* **105**, 026803 (2010).
- ¹⁰ S. V. Lotkhov, A. Kemppinen, S. Kafanov, J. P. Pekola, and A. B. Zorin, *Appl. Phys. Lett.* **95**, 112507 (2009).
- ¹¹ S. V. Lotkhov and A. B. Zorin, *Applied Physics Letters* **100**, 242601 (2012), <http://dx.doi.org/10.1063/1.4729417>.
- ¹² M. Watanabe and D. B. Haviland, *Phys. Rev. Lett.* **86**, 5120 (2001).
- ¹³ S. Corlevi, W. Guichard, F. W. J. Hekking, and D. B. Haviland, *Phys. Rev. B* **74**, 224505 (2006).
- ¹⁴ J. Oppenländer, C. Häussler, and N. Schopohl, *Phys. Rev. B* **63**, 024511 (2000).
- ¹⁵ C. Häussler, J. Oppenländer, and N. Schopohl, *Journal of Applied Physics* **89**, 1875 (2001).
- ¹⁶ S. V. Lotkhov, O.-P. Saira, J. P. Pekola, and A. B. Zorin, *New J. Phys.* **13**, 013040 (2011).
- ¹⁷ S. V. Lotkhov, B. Jalali-Jafari, and A. B. Zorin, *Applied Physics Letters* **108**, 172603 (2016), <http://dx.doi.org/10.1063/1.4948258>.
- ¹⁸ G. L. Ingold and Y. V. Nazarov, "Single charge tunneling," (Plenum Press, New York, 1992) p. 21.
- ¹⁹ A. Di Marco, V. F. Maisi, J. P. Pekola, and F. W. J. Hekking, *Phys. Rev. B* **88**, 174507 (2013).
- ²⁰ D. V. Averin and J. P. Pekola, *Phys. Rev. Lett.* **101**, 066801 (2008).
- ²¹ J. P. Pekola, O.-P. Saira, V. F. Maisi, A. Kemppinen, M. Möttönen, Y. A. Pashkin, and D. V. Averin, *Rev. Mod. Phys.* **85**, 1421 (2013).
- ²² O. Naaman and J. Aumentado, *Physical Review Letters* **96**, 100201 (2006).
- ²³ J. M. Martinis and M. Nahum, *Phys. Rev. B* **48**, 18316 (1993).
- ²⁴ J. M. Hergenrother, J. G. Lu, M. T. Tuominen, D. C. Ralph, and M. Tinkham, *Phys. Rev. B* **51**, 9407 (1995).
- ²⁵ O.-P. Saira, M. Möttönen, V. F. Maisi, and J. P. Pekola, *Phys. Rev. B* **82**, 155443 (2010).
- ²⁶ M. Covington, M. W. Keller, R. L. Kautz, and J. M. Martinis, *Phys. Rev. Lett.* **84**, 5192 (2000).
- ²⁷ O. P. Saira, *Electrostatic control of quasiparticle transport in superconducting hybrid nanostructures*, Ph.D. thesis, Aalto University (2013).
- ²⁸ D. C. Mattis and J. Bardeen, *Phys. Rev.* **111**, 412 (1958).
- ²⁹ N. R. Werthamer, *Phys. Rev.* **147**, 255 (1966).
- ³⁰ D. Pozar, *Microwave engineering*, 2nd ed. (John Wiley & Sons, 1998).
- ³¹ D. B. Haviland, K. Andersson, and P. Ågren, *Journal of Low Temperature Physics* **118**, 733 (2000).
- ³² V. Ambegaokar and A. Baratoff, *Phys. Rev. Lett.* **10**, 486 (1963).
- ³³ J. M. Martinis, K. B. Cooper, R. McDermott, M. Steffen, M. Ansmann, K. D. Osborn, K. Cicak, S. Oh, D. P. Pappas, R. W. Simmonds, and C. C. Yu, *Phys. Rev. Lett.* **95**, 210503 (2005).
- ³⁴ J. Hassel, P. Lähteenmäki, A. Timofeev, G. S. Paraoanu, and P. J. Hakonen, *PIERS Proceedings*, 484 (2013).